Chimica Techno Acta
published by Ural Federal University
eISSN 2411-1414
chimicatechnoacta.ru

ARTICLE
2023, vol. 10(2), No. 202310206
DOI: 10.15826/chimtech.2023.10.2.06

Novel co-doped protonic conductors $BaLa_{1.9}Sr_{0.1}In_{1.95}M_{0.05}O_{6.925}$ with layered perovskite structure

Anzhelika Bedarkova *, Nataliia Tarasova, Irina Animitsa, Ekaterina Abakumova, Irina Fedorova, Polina Cheremisina, Evgenia Verinkina

Institute of Hydrogen Energy, Ural Federal University, Ekaterinburg 620009, Russia
* Corresponding author: a.o.galisheva@urfu.ru

This paper belongs to a Regular Issue.

Abstract

Active development of electrochemical devices such as proton-conducting fuel cells and electrolyzers should ensure sustainable environmental development. An electrolyte material of a hydrogen-powered electrochemical device must satisfy a number of requirements, including high proton conductivity. Layered perovskites are a promising class of proton-conducting electrolytes. The cationic co-doping method has been successfully applied to well-known proton conductors with the classical perovskite structure ABO_3. However, the data on the application of this method to layered perovskites are limited. In this work, the bilayer perovskites $BaLa_{1.9}Sr_{0.1}In_{1.95}M_{0.05}O_{6.925}$ (M = Mg^{2+}, Ca^{2+}) were obtained and investigated for the first time. Cationic co-doping increases oxygen-ion and proton conductivity values.

Keywords

layered perovskite
oxygen-ion conductivity
proton conductivity
hydrogen energy
Ruddlesden-Popper structure

Received: 20.03.23
Revised: 06.04.23
Accepted: 06.04.23
Available online: 11.04.23

Key findings

- Cationic co-doping leads to an increase in proton conductivity of $BaLa_2In_2O_7$ values of up to ~0.8 orders of magnitude.
- The cationic co-doping strategy is a promising way to improve the transport properties of bilayer perovskites.

1. Introduction

Electrochemical devices such as proton-conducting fuel cells [1–3] and electrolyzers [4, 5] are in dire need of highly efficient materials with targeted properties including proton conductivity [6–8]. Active development and implementation of these devices as a part of the "hydrogen energy in everyday life" strategy should ensure sustainable environmental development [9–16]. The electrolyte material of a hydrogen-powered electrochemical device must satisfy a number of requirements, including high proton conductivity. One of the known ways to improve the conductivity is by co-doping of cationic sublattices of complex oxides. This method has been successfully applied to well-known proton conductors such as barium cerate-zirconates [17–22] and lanthanum scandates [23–26]. At the same time, the possibility of applying this method to a new class of proton-conducting materials, such as layered perovskites $AA'_nB_nO_{3n+1}$ [27], is currently under investigation.

The possibility of oxygen-ion transport in the monolayer perovskites $AA'BO_4$ was opened about ten years ago by Fujii et al. for compositions based on $BaNdInO_4$ [28–32] and by Troncoso et al. for compositions based on $SrLaInO_4$ [33–35]. The realisation of proton transport in the layered structures was demonstrated several years later for compositions based on BaLaInO4 [36]. Currently, a large class of materials with the monolayer perovskite structure Ba(Sr)La(Nd)In(Sc)O_4 [37–41] is described in terms of proton transport. The possibility of proton conductivity in bilayer $AA'_2B_2O_7$ perovskites such as on $BaLa_2In_2O_7$ [42–44], $BaNd_2In_2O_7$ [45] and $SrLa_2Sc_2O_7$ [46] and compositions based on them was described last year. It was shown that doping cationic sublattices can improve oxygen-ion and proton conductivity by up to 1.5 orders of magnitude [12]. It can be predicted that co-doping can also promote an increase in conductivity. In this work, we performed acceptor Sr^{2+}→La^{3+} and M^{2+}→In^{3+} (M = Mg^{2+}, Ca^{2+}) co-doping in the cationic sublattices of the bilayer perovskite $BaLa_2In_2O_7$. The doping effect on the proton conductivity was revealed.

2. Experimental

The compositions $BaLa_{1.9}Sr_{0.1}In_{1.95}Mg_{0.05}O_{6.925}$ and $BaLa_{1.9}Sr_{0.1}In_{1.95}Ca_{0.05}O_{6.925}$ were prepared by the solid state method. The powders of the starting reagents $BaCO_3$, $SrCO_3$, $CaCO_3$, MgO, La_2O_3, In_2O_3 were dried and used in stoichiometric amounts. The agate mortar was used for grinding. The compositions were heated after each grinding. The annealing was carried out in the temperature range of 800–1300 °C with 100 °C steps and 24 h dwell time at each step.

The phase identification of the obtained compositions was carried out using the Bruker Advance D8 Cu Kα diffractometer. The scanning electron microscope VEGA3 TESCAN was used to define the morphology of the samples. The thermogravimetric and mass spectrometric investigations were carried out using the NETZSCH STA 409 PC analyser equipped with the NETZSCH QMS 403C Aëolos mass spectrometer. Initially hydrated samples were used. The hydrated samples were obtained by slow cooling from 1100 to 150 °C (1 °C /min) under a flow of wet Ar.

The ceramic samples were prepared for the electrical properties studies. The powders were pressed into pellets and then sintered at 1300 °C for 24 h in dry air. The pellets had a relative density of ~92% (the density of the sintered samples was determined by the Archimedes method). The electrical conductivity was measured with an impedance spectrometer Z-1000P, Elins, RF. The investigations were carried out from 1000 to 200 °C at a cooling rate of 1°/min under dry air or dry Ar. The dry gas (air or Ar) was prepared by circulating the gas through P_2O_5 (pH_2O = $3.5\cdot10^{-5}$ atm). The wet gas (air or Ar) was obtained by bubbling the gas at room temperature first through distilled water and then through a saturated solution of KBr (pH_2O = $2\cdot10^{-2}$ atm).

3. Results and discussions

The phase attestation of the obtained compositions $BaLa_{1.9}Sr_{0.1}In_{1.95}Mg_{0.05}O_{6.925}$ and $BaLa_{1.9}Sr_{0.1}In_{1.95}Ca_{0.05}O_{6.925}$ was made using the X-ray diffraction method. The results of the Le Bail analysis of the XRD-data are presented in Figure 1.

Both samples are single phase and have orthorhombic symmetry with $P4_2/mnm$ space group. The introduction of bigger ions (Sr^{2+}) into La^{3+}-sublattice ($r_{La^{3+}}$ = 1.216 Å, $r_{Sr^{2+}}$ = 1.31 Å, $r_{In^{3+}}$ = 0.8 Å, $r_{Ca^{2+}}$ = 1.0 Å, $r_{Mg^{2+}}$ = 0.72 Å [47]) leads to an increase in the lattice parameter (Table 1). However, the additional introduction of Mg^{2+} and Ca^{2+} ions into the In^{3+} sublattice (co-doping) leads to a small decrease in the *c* lattice parameter and unit cell volume. The most probable reason for this is the local distortion of the crystal lattice due to the presence of several different cations in the cationic sublattices. In addition, the appearance of oxygen vacancies in the crystal lattice during acceptor doping also contributes to the distortion:

$$2SrO \xrightarrow{La_2O_3} 2Sr'_{La} + 2O_O^{\times} + V_O^{\bullet\bullet} \quad (1)$$

$$2Ca(Mg)O \xrightarrow{In_2O_3} 2Ca(Mg)'_{In} + 2O_O^{\times} + V_O^{\bullet\bullet} \quad (2)$$

Morphological analysis of the powder samples was carried out using scanning electron microscopy (SEM). The diameter of the grains was about ~2–5 μm (Figure 2).

The typical EIS-plots are presented in Figure 3. The conductivity values were calculated using resistance values taken at the intersection of the high-frequency semicircle with the abscissa axis. The capacitance values for these semicircles was ~ 10^{-12} F/cm, which corresponds to the resistance of the grain volume of the polycrystalline sample.

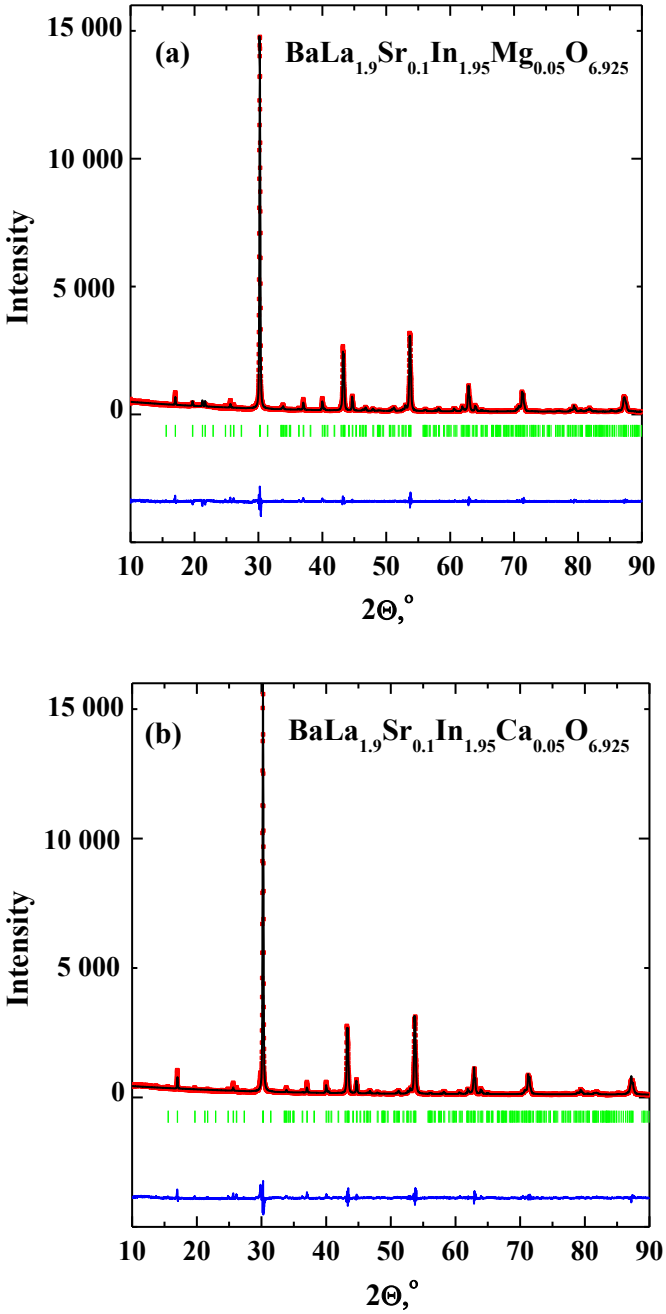

Figure 1 The results of XRD investigations for the compositions $BaLa_{1.9}Sr_{0.1}In_{1.95}Mg_{0.05}O_{6.925}$ (a) and $BaLa_{1.9}Sr_{0.1}In_{1.95}Ca_{0.05}O_{6.925}$ (b).

 DOI: 10.15826/chimtech.2023.10.2.06

Table 1 Lattice parameters, unit cell volume and water uptake for the investigated compositions.

Composition	*a*, *b* (Å)	*c* (Å)	V_{cell} (Å³)	Water uptake (mol)
$BaLa_2In_2O_7$	5.914(9)	20.846(5)	729.33(6)	0.17
$BaLa_{1.9}Sr_{0.1}In_2O_{6.95}$ [42]	5.916(3)	20.870(4)	730.51(8)	0.18
$BaLa_{1.9}Sr_{0.1}In_{1.95}Mg_{0.05}O_{6.925}$	5.916(3)	20.849(5)	729.78(6)	0.17
$BaLa_{1.9}Sr_{0.1}In_{1.95}Ca_{0.05}O_{6.925}$	5.916(4)	20.852(0)	729.89(9)	0.17

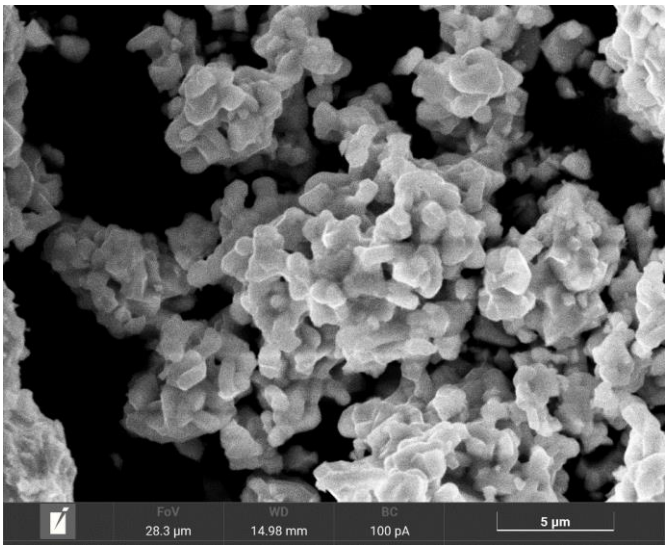

Figure 2 SEM result for the composition $BaLa_{1.9}Sr_{0.1}In_{1.95}Ca_{0.05}O_{6.925}$

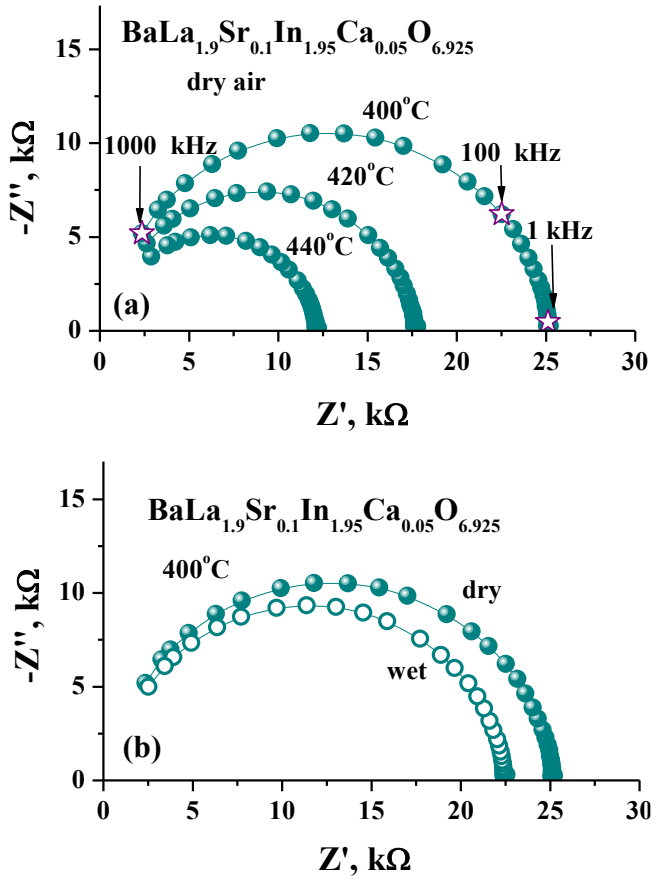

Figure 3 The EIS plots for the composition $BaLa_{1.9}Sr_{0.1}In_{1.95}Ca_{0.05}O_{6.925}$ obtained at 400 °C, 420 °C and 440 °C in dry air (a), and at 400 °C in dry and wet air (b).

The temperature dependences of the conductivity obtained under dry/wet air/Ar are presented in Figure 4a and Figure 4b for the compositions $BaLa_{1.9}Sr_{0.1}In_{1.95}Mg_{0.05}O_{6.925}$ and $BaLa_{1.9}Sr_{0.1}In_{1.95}Ca_{0.05}O_{6.925}$, respectively.

As can be seen, the conductivity values under dry Ar ($pO_2 \sim 10^{-5}$ atm) are lower than under dry air ($pO_2 = 0.21$ atm), indicating the hole contribution to the electrical conductivity:

$$V_o^{\bullet\bullet} + {}^1/_2\, O_2 \Leftrightarrow O_o^{\times} + 2h^{\bullet} \qquad (3)$$

The increase in water partial pressure leads to an increase in the conductivity values due to the formation of proton charge carriers:

$$h^{\bullet} + {}^1/_2\, H_2O + O_o^{\times} \Leftrightarrow {}^1/_4\, O_2 + (OH)_o^{\bullet}. \qquad (4)$$

$$V_o^{\bullet\bullet} + H_2O + O_o^{\times} \Leftrightarrow 2(OH)_o^{\bullet}. \qquad (5)$$

It should be noted that the conductivity values under wet air and wet Ar are very close at low temperatures, indicating the dominance of ion (proton) conductivity.

Figure 5 represents the comparison of the conductivity values for the co-doped compositions $BaLa_{1.9}Sr_{0.1}In_{1.95}Mg_{0.05}O_{6.925}$ and $BaLa_{1.9}Sr_{0.1}In_{1.95}Ca_{0.05}O_{6.925}$ compositions with undoped $BaLa_2In_2O_7$ and only Sr-doped $BaLa_{1.9}Sr_{0.1}In_2O_{6.95}$ compositions. As can be seen, co-doping leads to an increase in conductivity of up to one order of magnitude. The conductivity values increase in the $BaLa_2In_2O_7$ – $BaLa_{1.9}Sr_{0.1}In_{1.95}Mg_{0.05}O_{6.925}$ – $BaLa_{1.9}Sr_{0.1}In_{1.95}Ca_{0.05}O_{6.925}$ – $BaLa_{1.9}Sr_{0.1}In_2O_{6.95}$ series, which correlates with the increase in the lattice parameter and unit cell volume.

The activation energy values for the oxygen-ion and proton conductivities were calculated and are presented in Table 2. As can be seen, the activation energy of the oxygen-ion conductivity of the co-doped compositions $BaLa_{1.9}Sr_{0.1}In_{1.95}Mg_{0.05}O_{6.925}$ and $BaLa_{1.9}Sr_{0.1}In_{1.95}Ca_{0.05}O_{6.925}$ is lower than for undoped $BaLa_2In_2O_7$ and only Sr-doped $BaLa_{1.9}Sr_{0.1}In_2O_{6.95}$ compositions. A more detailed study of these samples is required to explain this fact.

Table 2 Activation energy values for the oxygen-ion and proton conductivities for the investigated compositions.

Composition	E_a for O^{2-}(eV)	E_a for H^+(eV)
$BaLa_2In_2O_7$	0.80	0.63
$BaLa_{1.9}Sr_{0.1}In_2O_{6.95}$ [42]	0.80	0.57
$BaLa_{1.9}Sr_{0.1}In_{1.95}Mg_{0.05}O_{6.925}$	0.72	0.75
$BaLa_{1.9}Sr_{0.1}In_{1.95}Ca_{0.05}O_{6.925}$	0.77	0.75

DOI: 10.15826/chimtech.2023.10.2.06

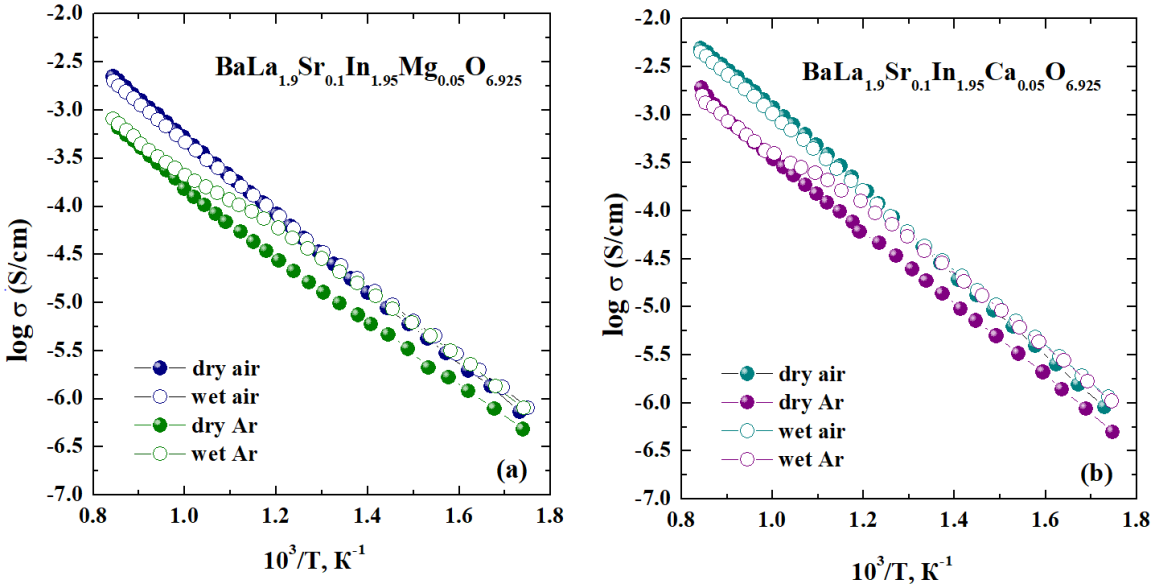

Figure 4 The temperature dependences for the compositions $BaLa_{1.9}Sr_{0.1}In_{1.95}Mg_{0.05}O_{6.925}$ (a) and $BaLa_{1.9}Sr_{0.1}In_{1.95}Ca_{0.05}O_{6.925}$ (b).

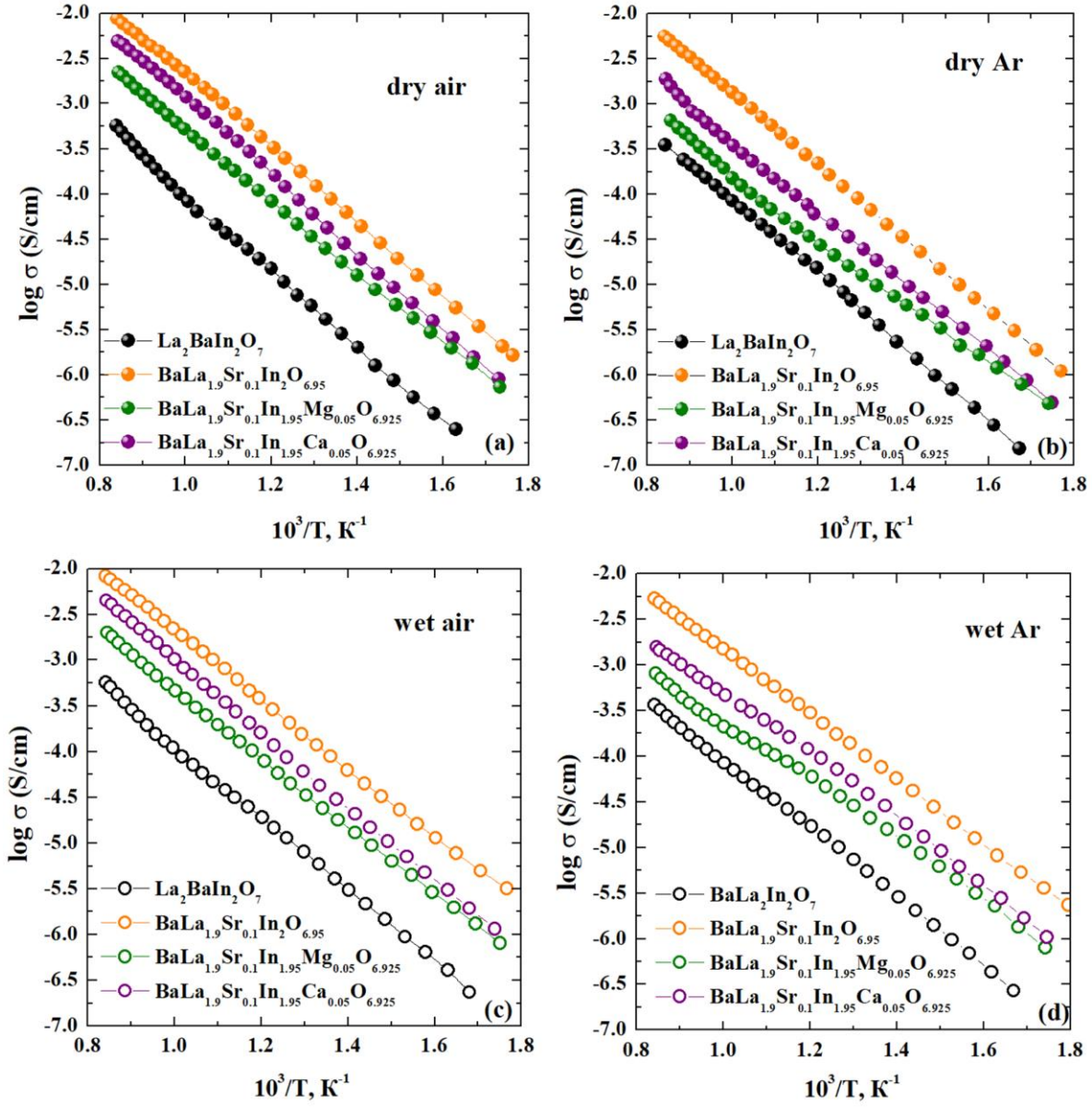

Figure 5 The temperature dependences of electrical conductivity for the compositions $BaLa_2In_2O_7$, $BaLa_{1.9}Sr_{0.1}In_{1.95}Mg_{0.05}O_{6.925}$, $BaLa_{1.9}Sr_{0.1}In_{1.95}Ca_{0.05}O_{6.925}$, $BaLa_{1.9}Sr_{0.1}In_2O_{6.95}$ [42] in dry air (a), dry Ar (b), wet air (c), wet Ar (d).

 DOI: 10.15826/chimtech.2023.10.2.06

It should be noted that the co-doped $BaLa_{1.9}Sr_{0.1}In_{1.95}Mg_{0.05}O_{6.925}$ and $BaLa_{1.9}Sr_{0.1}In_{1.95}Ca_{0.05}O_{6.925}$ compositions contain 50% more oxygen vacancies than the $BaLa_{1.9}Sr_{0.1}In_2O_{6.95}$ composition. We can conclude that the change in the geometric characteristic of the unit cell volume has the most significant effect on the conductivity value than a change in the concentration of oxygen vacancies.

The temperature dependences of the proton conductivities, calculated as the difference between the ionic conductivity under wet conditions (wet Ar) and dry conditions (dry Ar), are presented in Figure 6. The values of the activation energy of the proton conductivity calculated from Figure 6 are given in Table 2. The activation energy decreases from 0.63 eV for the undoped $BaLa_2In_2O_7$ composition to 0.57 eV for the $BaLa_{1.9}Sr_{0.1}In_2O_{6.95}$ composition by introducing only strontium as a dopant. Interestingly, co-doping leads to a decrease in the values of the activation energy of proton conduction.

The same regularity of increase in conductivity values for the doped compositions is observed. The values of the proton concentrations are required for the correct analysis of these dependences.

Figure 7 shows the results of thermogravimetry (TG), mass spectrometry (MS) and differential scanning calorimetry (DSC) analysis for the $BaLa_{1.9}Sr_{0.1}In_{1.95}Ca_{0.05}O_{6.925}$ composition. Mass loss occurs at the temperatures below 700 °C (TG curve) and is solely due to the release of water (MS(H_2O) curve). The values of water uptake are close for all doped $BaLa_{1.9}Sr_{0.1}In_{1.95}M_{0.05}O_{6.925}$ (M = Mg, Ca), $BaLa_{1.9}Sr_{0.1}In_2O_{6.95}$ and undoped $BaLa_2In_2O_7$ compositions and are about ~ 0.17–0.18 mol of water per formula unit (Table 1). In other words, the proton concentration (c_{H^+}) is close for all compositions. Consequently, the increase in proton conductivity $(\sigma_{H^+})_x$ is due to the increase in proton mobility (μ_{H^+}):

$$\sigma_{H^+} = z \cdot e \cdot \mu_{H^+} \cdot c_{H^+}. \quad (6)$$

We conclude that co-doping positively affects the ionic conductivity of $BaLa_2In_2O_7$. An increase in lattice parameters leads to facilitation of oxygen-ion transport, which, in turn, leads to an increase in oxygen-ion conductivity. At the same time, co-doping also leads to an increase in proton conductivity, probably due to an increase in proton mobility. The proton conductivity values for co-doped compositions are $2.9 \cdot 10^{-6}$ S/cm and $5.4 \cdot 10^{-6}$ S/cm at 400 °C for the compositions $BaLa_{1.9}Sr_{0.1}In_{1.95}Mg_{0.05}O_{6.925}$ and $BaLa_{1.9}Sr_{0.1}In_{1.95}Ca_{0.05}O_{6.925}$, respectively.

The comparison of the electrical conductivity values obtained in wet air for the undoped $BaLa_2In_2O_7$, monodoped $BaLa_{1.9}Sr_{0.1}In_2O_{6.95}$ and co-doped $BaLa_{1.9}Sr_{0.1}In_{1.95}M_{0.05}O_{6.925}$ (M = Mg, Ca) compositions with known proton conductors such as doped barium and strontium ceramics is shown in Figure 8.

The conductivity of the studied compositions under wet conditions is lower than that of doped barium and strontium cerates. Nevertheless, acceptor doping can increase conductivity values by up to ~1.5 orders of magnitude.

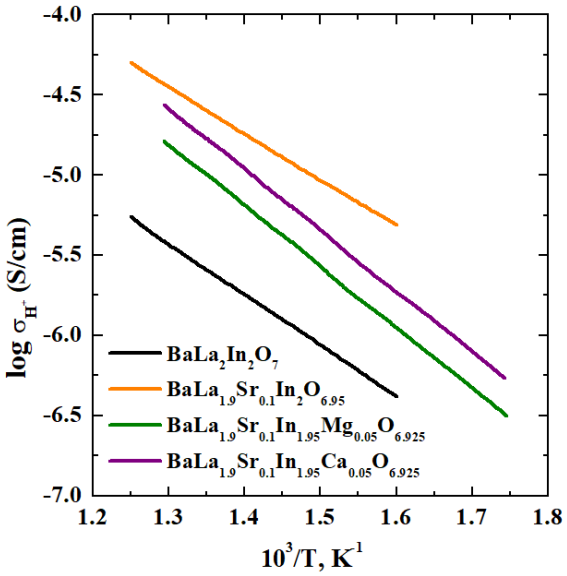

Figure 6 The temperature dependences of protonic conductivity for the compositions $BaLa_2In_2O_7$, $BaLa_{1.9}Sr_{0.1}In_{1.95}Mg_{0.05}O_{6.925}$, $BaLa_{1.9}Sr_{0.1}In_{1.95}Ca_{0.05}O_{6.925}$, $BaLa_{1.9}Sr_{0.1}In_2O_{6.95}$ [42]

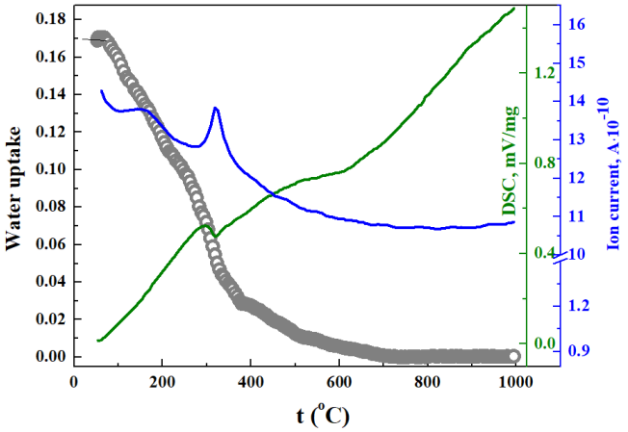

Figure 7 The results of TG, DSC and MS(H_2O) investigations for the composition $BaLa_{1.9}Sr_{0.1}In_{1.95}Ca_{0.05}O_{6.925}$.

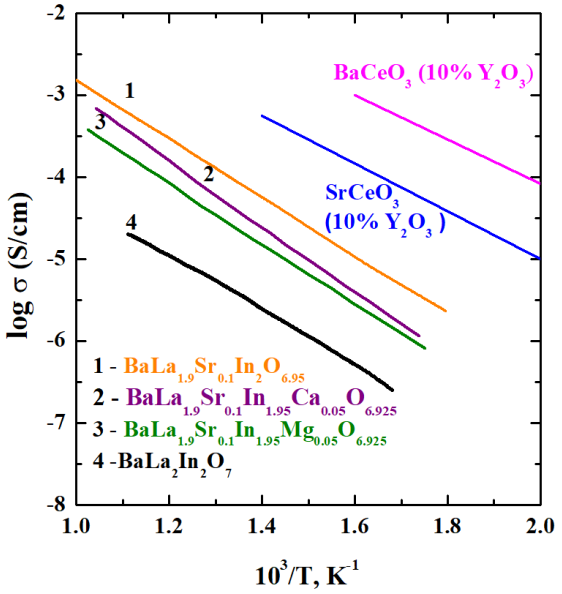

Figure 8 The temperature dependences of conductivity obtained in wet air for compositions $BaLa_{1.9}Sr_{0.1}In_2O_{6.95}$ [42], $BaLa_{1.9}Sr_{0.1}In_{1.95}Mg_{0.05}O_{6.925}$, $BaLa_{1.9}Sr_{0.1}In_{1.95}Ca_{0.05}O_{6.925}$, $BaLa_2In_2O_7$, $BaCeO_3$ (10 mol.% Y_2O_3) [48], $SrCeO_3$(10 mol.% Y_2O_3) [48]

 DOI: 10.15826/chimtech.2023.10.2.06

4. Limitations

Firstly, we have some limitations in the measurement of electrical conductivity. The maximum frequency measured with the Elins Z-1000P impedance spectrometer is 1000 kHz. The measurement of the conductivity at higher frequencies will give a more accurate representation of the EIS-plots at T > 500 °C.

Secondly, a full explanation of the activation energy values obtained for co-doped compositions is difficult at this stage of the study. For the $BaLa_2In_2O_7$ composition, which is co-doped in the A and B sublattices, a more detailed study of the ion transport mechanisms is required.

Thirdly, doping the $BaLa_2In_2O_7$ composition leads to an increase in electrical conductivity of up to 1.5 orders of magnitude. However, the conductivity of the compositions studied in this article is lower than that of doped barium and strontium ceramics.

5. Conclusions

In this paper, we performed acceptor $Sr^{2+}\rightarrow La^{3+}$ and $M^{2+}\rightarrow In^{3+}$ (M = Mg^{2+}, Ca^{2+}) co-doping in the cationic sublattices of the bilayer perovskite $BaLa_2In_2O_7$. The bilayer perovskites $BaLa_{1.9}Sr_{0.1}In_{1.95}Mg_{0.05}O_{6.925}$ and $BaLa_{1.9}Sr_{0.1}In_{1.95}Ca_{0.05}O_{6.925}$ were obtained and investigated for the first time. The phase attestation, morphology, possibility of water uptake and electrical conductivity were investigated and discussed. The doping effect on the oxygen-ion and proton conductivity was revealed. It was shown that cationic co-doping leads to an increase in proton conductivity values of up to ~0.8 orders of magnitude.

• Supplementary materials

None.

• Funding

The research funding from the Ministry of Science and Higher Education of the Russian Federation (Ural Federal University Program of Development within the Priority-2030 Program) is gratefully acknowledged.

• Acknowledgments

None.

• Author contributions

Conceptualization: N.T., I.A.
Data curation: A.B., N.T.
Methodology: N.T., I.A.
Investigation: A.B., E.A., I.F., P.C., E.V.
Validation: A.B., N.T.
Visualization: A.B., E.A., N.T.
Writing – original draft: N.T.
Writing – review & editing: N.T., A.B.,

• Conflict of interest

The authors declare no conflict of interest.

• Additional information

Author IDs:
Natalia Tarasova, Scopus ID 37047923700;
Anzhelika Bedarkova, Scopus ID 57195274932;
Irina Animitsa, Scopus ID 6603520951.

Website:
Ural Federal University, https://urfu.ru/en.

References

1. Zhang W, Hu YH. Progress in proton-conducting oxides as electrolytes for low-temperature solid oxide fuel cells: From materials to devices. Energy Sci Eng. 2021;9:984–1011. doi:10.1002/ese3.886
2. Nayak AP, Sasmal A. Recent advance on fundamental properties and synthesis of barium zirconate for proton conducting ceramic fuel cell. J Cleaner Product. 2023;386:135827. doi:10.1016/j.jclepro.2022.135827
3. Guo R, He T. High-entropy perovskite electrolyte for protonic ceramic fuel cells operating below 600 °C. ACS Mater Lett. 2022;4:1646–1652. doi:10.1021/acsmaterialslett.2c00542
4. Wang C, Li Z, Zhao S, Xia L, Zhu M, Han M, Ni M. Modelling of an integrated protonic ceramic electrolyzer cell (PCEC) for methanol synthesis. J Power Sources. 2023;559:232667. doi:10.1016/j.jpowsour.2023.232667
5. Ji HI, Lee JH, Son JW, Yoon KJ, Yang S, Kim BK. Protonic ceramic electrolysis cells for fuel production: A brief review. J Korean Ceram Soc. 2020;57:480–494. doi:10.1007/s43207-020-00059-4
6. Liu F, Ding D, Duan C. Protonic ceramic electrochemical cells for synthesizing sustainable chemicals and fuels. Adv Sci. 2023;10:2206478. doi:10.1002/advs.202206478
7. Kim D, Bae KT, Kim KJ, Im H-N, Jang S, Oh S, Lee SW, Shin TH, Lee KT. High-performance protonic ceramic electrochemical cells. ACS Energy Lett. 2022;7:2393–2400. doi:10.1021/acsenergylett.2c01370
8. Tian H, Luo Z, Song Y, Zhou Y, Gong M, Li W, Shao Z, Liu M, Liu X. Protonic ceramic materials for clean and sustainable energy: Advantages and challenges. Int Mater Rev. 2022;0:1–29. doi:10.1080/09506608.2022.2068399
9. Corigliano O, Pagnotta L, Fragiacomo P. On the technology of solid oxide fuel cell (SOFC) energy systems for stationary power generation: A review. Sustain. 2022;14:15276. doi:10.3390/su142215276
10. Kumar SS, Lim H. An overview of water electrolysis technologies for green hydrogen production. Energy Rep. 2022;8:13793–13813. doi:10.1016/j.egyr.2022.10.127
11. Huang L, Huang X, Yan J, Liu Y, Jiang H, Zhang H, Tang J, Liu Q. Research progresses on the application of perovskite in adsorption and photocatalytic removal of water pollutants. J Hazard Mater. 2023;442:130024. doi:10.1016/j.jhazmat.2022.130024
12. Tarasova N. Layered perovskites $BaLn_nIn_nO_{3n+1}$ (n = 1, 2) for electrochemical applications: A mini review. Membran. 2023;13:34. doi:10.3390/membranes13010034
13. Zvonareva IA, Medvedev DA. Proton-conducting barium stannate for high-temperature purposes: A brief review. J Eur Ceram Soc. 2023;43:198–207. doi:10.1016/j.jeurceramsoc.2022.10.049
14. Aminudin MA, Kamarudin SK, Lim BH, Majilan EH, Masdar MS, Shaari N. An overview: Current progress on hydrogen

fuel cell vehicles. Int J Hydrog Energy. 2023;48:4371–4388. doi:10.1016/j.ijhydene.2022.10.156
15. Liu F, Fang L, Diercks D, Kazempoor P, Duan C. Rationally designed negative electrode for selective CO_2-to-CO conversion in protonic ceramic electrochemical cells. Nano Energy. 2022;102:107722. doi:10.1016/j.nanoen.2022.107722
16. Liu F, Duan C. Direct-hydrocarbon proton-conducting solid oxide fuel cells. Sustain. 2021;13:4736. doi:10.3390/su13094736
17. Nayak AK, Sasmal A. Recent advance on fundamental properties and synthesis of barium zirconate for proton conducting ceramic fuel cell. J Clean Prod. 2023;386:135827. doi:10.1016/j.jclepro.2022.135827
18. Qiao Z, Li S, Li Y, Xu N, Xiang K. Structure, mechanical properties, and thermal conductivity of $BaZrO_3$ doped at the A-B site. Ceram Int. 2022;48;12529–12536. doi:10.1016/j.ceramint.2022.01.120
19. Guo R, Li D, Guan R, Kong D, Cui Z, Zhou Z, He T. Sn–Dy–Cu triply doped $BaZr_{0.1}Ce_{0.7}Y_{0.2}O_{3-\delta}$: A chemically stable and highly proton-conductive electrolyte for low-temperature solid oxide fuel cells. ACS Sustain Chem Eng. 2022;10:5352–5362. doi:10.1021/acssuschemeng.2c00807
20. Gu Y, Luo G, Chen Z, Huo Y, Wu F. Enhanced chemical stability and electrochemical performance of $BaCe_{0.8}Y_{0.1}Ni_{0.04}Sm_{0.06}O_{3-\delta}$ perovskite electrolytes as proton conductors. Ceram Int. 2022;48:10650–10658. doi:10.1016/j.ceramint.2021.12.279
21. Medvedev DA. Current drawbacks of proton-conducting ceramic materials: How to overcome them for real electrochemical purposes. Curr Opin Green Sustain Chem. 2021;32:100549. doi:10.1016/j.cogsc.2021.100549
22. Kasyanova AV, Zvonareva IA, Tarasova NA, Bi L, Medvedev DA, Shao Z. Electrolyte materials for protonic ceramic electrochemical cells: Main limitations and potential solutions. Mater Rep Energy. 2022;2:100158. doi:10.1016/j.matre.2022.100158
23. Lybye D, Poulsen FW, Mogensen M. Conductivity of A- and B-site doped $LaAlO_3$, $LaGaO_3$, $LaScO_3$ and $LaInO_3$ perovskites. Solid State Ion. 2000;128:91–103. doi:10.1016/S0167-2738(99)00337-9
24. Stroeva AY, Gorelov VP, Balakireva VB. Conductivity of $La_{1-x}Sr_xSc_{1-y}Mg_yO_{3-\alpha}$ (x = y = 0.01–0.20) in reducing atmosphere. Russ J Electrochem. 2010;46:784–788. doi:10.1134/S1023193510070116
25. Ito N, Matsumoto H, Kawasaki Y, Okada S, Ishihara T. The effect of Zn addition to $La_{1-x}Sr_xScO_{3-\delta}$ systems as a B-site dopant. Chem Lett. 2009;38:582–583. doi:10.1246/cl.2009.582
26. Kato H, Iguchi F, Yugami H. Compatibility and performance of $La_{0.675}Sr_{0.325}Sc_{0.99}Al_{0.01}O_3$ perovskite-type oxide as an electrolyte material for SOFCs. Electrochem. 2014;82:845–850. doi:10.5796/electrochemistry.82.845
27. Ruddlesden SN, Popper P. The compound $Sr_3Ti_2O_7$ and its structure. Acta Cryst. 1958;11:54–55. doi:10.1107/S0365110X58000128
28. Fujii K, Esaki Y, Omoto K, Yashima M, Hoshikawa A, Ishigaki T, Hester JR. New perovskite-related structure family of oxide-ion conducting materials $NdBaInO_4$. Chem Mater. 2014;26:2488–2491. doi:10.1021/cm500776x
29. Fujii K, Shiraiwa M, Esaki Y, Yashima M, Kim SJ, Lee S. Improved oxide-ion conductivity of $NdBaInO_4$ by Sr doping. J Mater Chem A. 2015;3:11985. doi:10.1039/c5ta01336d
30. Ishihara T, Yan Yu, Sakai T, Ida S. Oxide ion conductivity in doped $NdBaInO_4$. Solid State Ion. 2016;288:262. doi:10.1016/j.ssi.2016.01.011
31. Yang X, Liu S, Lu F, Xu J, Kuang X. Acceptor doping and oxygen vacancy migration in layered perovskite $NdBaInO_4$-based mixed conductors. J Phys Chem C. 2016;120:6416–6426. doi:10.1021/acs.jpcc.6b00700
32. Fijii K, Yashima M. Discovery and development of $BaNdInO_4$—A brief review. J Ceram Soc Jpn. 2018;126:852–859. doi:10.2109/jcersj2.18110
33. Troncoso L, Alonso JA, Aguadero A. Low activation energies for interstitial oxygen conduction in the layered perovskites $La_{1+x}Sr_{1-x}InO_{4+d}$. J Mater Chem A. 2015;3:17797–17803. doi:10.1039/c5ta03185k
34. Troncoso L, Alonso JA, Fernández-Díaz MT, Aguadero A. Introduction of interstitial oxygen atoms in the layered perovskite $LaSrIn_{1-x}B_xO_{4+\delta}$ system (B=Zr, Ti). Solid State Ion. 2015;282:82–87. doi:10.1016/j.ssi.2015.09.014
35. Troncoso L, Mariño C, Arce MD, Alonso JA. Dual oxygen defects in layered $La_{1.2}Sr_{0.8-x}Ba_xInO_{4+d}$ (x = 0.2, 0.3) oxide-ion conductors: A neutron diffraction study. Mater. 2019;12:1624. doi:10.3390/ma12101624
36. Tarasova N, Animitsa I, Galisheva A, Korona D. Incorporation and conduction of protons in Ca, Sr, Ba-doped $BaLaInO_4$ with Ruddlesden-Popper structure. Mater. 2019;12:1668. doi:10.3390/ma12101668
37. Troncoso L, Arce MD, Fernández-Díaz MT, Mogni LV, Alonso JA. Water insertion and combined interstitial-vacancy oxygen conduction in the layered perovskites $La_{1.2}Sr_{0.8-x}Ba_xInO_{4+\delta}$. New J Chem. 2019;43:6087–6094. doi:10.1039/C8NJ05320K
38. Zhou Y, Shiraiwa M, Nagao M, Fujii K, Tanaka I, Yashima M, Baque L, Basbus JF, Mogni LV, Skinner SJ. Protonic conduction in the $BaNdInO_4$ structure achieved by acceptor doping. Chem Mater. 2021;33:2139–2146. doi:10.1021/acs.chemmater.0c04828
39. Shiraiwa M, Kido T, Fujii K, Yashima M. High-temperature proton conductors based on the (110) layered perovskite $BaNdScO_4$. J Mat Chem A. 2021;9:8607. doi:10.1039/D0TA11573H
40. Tarasova N, Animitsa I. Materials $A^{II}LnInO_4$ with Ruddlesden-Popper structure for electrochemical applications: Relationship between ion (oxygen-ion, proton) conductivity, water uptake and structural changes. Mater. 2022;15:114. doi:10.3390/ma15010114
41. Tarasova N, Animitsa I, Galisheva A, Medvedev D. Layered and hexagonal perovskites as novel classes of proton-conducting solid electrolytes: A focus review. Electrochem. Mater Technol. 2022;1:20221004. doi:10.15826/elmattech.2022.1.004
42. Tarasova N, Galisheva A, Animitsa I, Abakumova E, Belova K, Kreimesh H. Novel high conductive ceramic materials based on two-layer perovskite $BaLa_2In_2O_7$. Int J Mol Sci. 2022;23:12813. doi:10.3390/ijms232112813
43. Tarasova N, Bedarkova A, Animitsa I, Belova K, Abakumova E, Cheremisina P, Medvedev D. Oxygen ion and proton transport in alkali-earth doped layered perovskites based on $BaLa_2In_2O_7$. Inorg. 2022;10:161. doi:10.3390/inorganics10100161
44. Tarasova N, Bedarkova A, Animitsa I, Verinkina E. Synthesis, hydration processes and ionic conductivity of novel gadolinium-doped ceramic materials based on layered perovskite $BaLa_2In_2O_7$ for electrochemical purposes. Processes. 2022;10:2536. doi:10.3390/pr10122536
45. Tarasova N, Bedarkova A, Animitsa I, Abakumova E. Cation and oxyanion doping of layered perovskite $BaNd_2In_2O_7$: Oxygen-ion and proton transport. Int J Hydrog Energy. 2022, in press. doi:10.1016/j.ijhydene.2022.11.172
46. Tarasova N, Bedarkova A, Animitsa I, Abakumova E, Gnatyuk V, Zvonareva I. Novel protonic conductor $SrLa_2Sc_2O_7$ with layered structure for electrochemical devices. Mater. 2022;15:8867. doi:10.3390/ma15248867
47. Shannon RD. Revised effective ionic radii and systematic studies of interatomic distances in halides and chalcogenides. Acta Cryst. 1976;A32:751–67. doi:10.1107/S0567739476001551
48. Kreuer KD. Proton-conducting oxides. Annu Rev Mater Res. 2003;33:333–359. doi:10.1146/annurev.matsci.33.022802.09182

 DOI: 10.15826/chimtech.2023.10.2.06